INORGANIC CHEMISTRY FRONTIERS

RESEARCH ARTICLE

View Article Online
View Journal | View Issue

Cite this: *Inorg. Chem. Front.*, 2023, **10**, 5488

$KNa_2La_2(BO_3)_3$: a shortite-type lanthanide borate exhibiting strong nonlinear optical activity induced by isolated $[BO_3]$ triangles and distorted $[LaO_9]$ polyhedra†

Jie Song,[a] Conggang Li, *[a] Jinmiao Jiao,[a] Yuheng She,[a] Wenli Zhao,[a] Fei Liang, *[b] Ning Ye,[a] Zhanggui Hu*[a] and Yicheng Wu[a]

Received 30th May 2023,
Accepted 11th August 2023

DOI: 10.1039/d3qi01004j

rsc.li/frontiers-inorganic

The targeted synthesis of ultraviolet (UV) nonlinear optical (NLO) materials with strong second-harmonic generation (SHG) activity and wide transparency window remains a formidable challenge. Herein, a prospective rare-earth borate UV NLO crystal, $KNa_2La_2(BO_3)_3$, was extracted by spontaneous crystallization using a flux method. The title compound crystallizes into the acentric orthorhombic space group *Amm*2 (no. 38), analogous to those of shortite, and affords a three-dimensional framework built from planar $[BO_3]$ triangles and distorted $[LaO_9]$ motifs. The optical spectroscopy analyses demonstrate that $KNa_2La_2(BO_3)_3$ displays a short cutoff edge of 212 nm, accompanied by a wide band gap of 5.3 eV. Notably, it achieves an enhanced phase-matching SHG efficiency of 2.6 × KDP, comparable with those of the other NLO rare earth borate oxide crystals. Besides, theoretical analyses revealed that the optimized optical polarizability of $KNa_2La_2(BO_3)_3$ is predominantly ascribed to the cooperative effects of the isolated $[BO_3]$ and distortive $[LaO_9]$ structural units. This finding showcases a promising UV NLO crystal and sheds light on further exploration of rare earth metal-based NLO materials with fascinating performances.

Introduction

Second-order nonlinear optical (NLO) crystals have been widely used in laser science and technology, as they possess the capability of frequency conversion that is able to expand the wavelength range of common laser sources to the spectral region.[1,2] In particular, those used in the ultraviolet (UV) range (λ < 400 nm) play a pivotal role in the fields of optoelectronics, such as laser micromanufacturing, information storage, biological tissue imaging, and photoemission spectroscopy.[3–6] Consequently, considerable research has been devoted to designing and fabricating potential UV NLO materials.

The primary requirement for targeting a NLO material is that it must be crystallographically acentric. The efficient approach to predesigning acentric structures is to introduce NLO-active chromophores as fundamental building blocks,[7] such as the second-order Jahn–Teller (SOJT) distortive cations with local asymmetric coordination (*e.g.*, Ti^{4+}, Nb^{5+}, Mo^{6+}),[8] stereo-chemically active lone-pair cations (*e.g.*, Bi^{3+}, Te^{4+}, Sn^{2+}, *etc.*),[9] or π-conjugated oxyanions (*e.g.*, $[BO_3]^{3-}$, $[CO_3]^{2-}$, $[NO_3]^{-}$).[10] Although, the compounds containing the SOJT distorted cations are widely utilized to increase the possibility of generating favorable microscopic polarizability when arranged in an optimal manner, nevertheless, they can also cause the UV absorption cutoff edge of the material to be adversely red-shifted, thus hardly maintaining adequate transmittance over the UV region.[11] Compared with the situation above, borates have attracted considerable research interest and are consistently viewed as competitive candidates for UV NLO crystals with intriguing performances because the optically active π-conjugated B–O units adopt coplanar configurations that promote a wide transparency window down to the UV region and large microscopic second-order hyperpolarizabilities.[12,13] Accordingly, this served as inspiration for the discovery of a wide variety of UV NLO materials with $[BO_3]$ triangles, including $KBe_2BO_3F_2$,[14] $Li_4Sr(BO_3)_2$,[15] $K_3B_6O_{10}Cl$,[16] $Ba_4B_{11}O_{20}F$,[17] and $Ba_3Mg_3(BO_3)_3F_3$.[18] Although the development of laser technology has been facilitated by these crystals, exploiting

[a]*Tianjin Key Laboratory of Functional Crystal Materials, Institute of Functional Crystal, Tianjin University of Technology, Tianjin 300384, China. E-mail: cgli@email.tjut.edu.cn, hu@mail.ipc.ac.cn*
[b]*State Key Laboratory of Crystal Materials and Institute of Crystal Materials, Shandong University, Jinan 250100, China. E-mail: liangfei@sdu.edu.cn*

†Electronic supplementary information (ESI) available: Additional crystallographic data, crystals, varied temperature PXRD, EDS analysis, calculated birefringence of KNLBO. CCDC 2265827. For ESI and crystallographic data in CIF or other electronic format see DOI: https://doi.org/10.1039/d3qi01004j

new NLO materials that have simultaneously enhanced second harmonic generation (SHG) efficiency and high UV transparency remains an enormous challenge.

According to previous studies, the enriched structural chemistry of lanthanide metal ions enables them to produce local asymmetric coordination environments, similar to the second-order SOJT distortions.[19] In particular, some rare-earth metal ions with closed-shell electron systems, such as Y^{3+}, Sc^{3+}, La^{3+}, and Lu^{3+}, inhibit the intrinsic d–d or f–f electronic transitions and thus give sufficient optical transparency in the UV window, as seen in compounds like $La_2CaB_{10}O_{19}$,[20] $K_5Mg_2La_3(BO_3)_6$,[21] and $K_7CdRE_2B_{15}O_{30}$ (RE = Sc, Y, Gd, Lu).[22]

Motivated by these, we focused special attention on the rare-earth metal–borate system in order to fabricate novel UV NLO crystals with improved optical properties. Our design ideas are mainly considered as follows: (i) La^{3+} has a large ionic radius among the rare earth metals and exhibits flexible coordination environments,[23] which is preferable to produce localized structural distortion, and it is chosen for this work as the rare-earth metal ion; and (ii) the violet-shifting of the UV absorption edge and widening of the band gap can be successfully induced by the introduction of light alkali metal ions without d–d or f–f electronic transitions. For example, the lanthanide borate NLO crystal $Na_3La_2(BO_3)_3$ features an enlarged SHG intensity (2 × KDP) and a short UV absorption edge of 213 nm.[24] Consider that isomorphism can occur between sodium and potassium.[25] Therefore, by introducing the light alkali metal ions K^+ and Na^+, the first effective fabrication of a new rare-earth borate NLO crystal, $KNa_2La_2(BO_3)_3$ (KNLBO), was experimentally accomplished using the $[BO_3]$ triangle system in combination with the flexible coordinated La^{3+} rare earth metal ion. KNLBO crystallizes into the non-centrosymmetric *Amm*2 (no. 38) space group. Its arrangement mode of $[BO_3]$ planar triangles is analogous to that of $[CO_3]$ in carbonates, like $Na_2Ca_2(CO_3)_3$, which affords a typical shortite structure.[26] As expected, the title compound fully achieved the coexistence of strong phase-matching SHG activity (2.6 × KDP) and short UV cut-off edge (212 nm), along with a broad band gap (5.3 eV), which indicates that KNLBO is a potential UV NLO material. Herein, we present its synthesis, crystal structure, thermal behavior, optical properties, and theoretical analyses.

Experimental

Polycrystalline synthesis

Polycrystalline KNLBO was synthesized using the starting materials K_2CO_3 (Sinopharm, 99.9%), Na_2CO_3 (Sinopharm, 99.9%), La_2O_3 (Sinopharm, 99.9%), and B_2O_3 (Sinopharm, 99.9%) with stoichiometric ratios *via* a standard solid-state reaction approach. Initially, the mixture contained within the crucible was inserted in a muffle furnace and was preheated at 450 °C for 24 h. Afterward, the products were sintered at no less than 700 °C for 72 h with several intermittent regrindings. Then, the target polycrystalline compound KNLBO was experimentally prepared, and its purity was further supported by powder X-ray diffraction analyses.

Powder X-ray diffraction (PXRD)

PXRD analyses of the polycrystalline KNLBO were carried out through a conventional Rigaku SmartLab 9 kW diffractometer with monochromatized Cu Kα radiation (λ = 1.5418 Å) recorded ranging from 10 to 70° at a step size of 0.01° with a step time of 0.3 s at room temperature.

Second-harmonic generation (SHG) characterization

On the basis of the Kurtz–Perry approach,[27] the polycrystalline powder SHG measurements of KNLBO were implemented under an incident laser beam (λ = 1064 nm) emitted from a Q-switched Nd:YAG laser at ambient temperatures. Because the powder SHG intensity depends on the particle size range of powder, the pure polycrystalline sample of KNLBO was screened and graded into the following several different particle ranges: 21–51, 51–74, 74–105, 105–125, 125–177 and 177–210 μm. Meanwhile, the standard polycrystalline samples KDP (KH_2PO_4) and LBO (LiB_3O_5) were also sieved into the corresponding size ranges to conduct pertinent comparisons.

Thermal properties

Differential scanning calorimetry (DSC) combined with thermogravimetric analyses (TGA) for the target compounds was conducted on a NETZSCH STA 449F5 TG/DSC thermal analyzer. The polycrystalline KNLBO was simultaneously heated up to 1200 °C at a rate of 10 °C min^{-1} and then slowly cooled down to ambient temperature under a N_2 atmosphere.

Crystal preparation and structural determination

KNLBO single crystals were extracted through a spontaneous crystallization technique. By using B_2O_3–K_2CO_3 as the fluxes, the target crystals were experimentally prepared. Single-crystal XRD analyses were conducted to process the structure of KNLBO. The crystallographic data were collected by employing a Bruker D8 VENTURE CMOS X-ray source with Mo Kα radiation (λ = 0.71073 Å). Multi-scan absorption corrections were applied according to the APEX III software. Based on the SHELXTL crystallography software system, the preliminary crystal model was processed and further refined by direct methods.[28] The structural symmetry of KNLBO was identified by employing the PLATON program.[29] The detailed crystallographic data on the atomic coordinates, equivalent isotropic displacement parameters, bond distances and angles, and anisotropic displacement parameters are presented in Tables S1 and S2.†

Energy-dispersive spectroscopy

The energy-dispersive spectroscopy (EDS) analyses of the target compound were carried out with a field emission scanning electron microscope (FEI Quanta FEG 250). To obtain elemental mapping images, the field-emission scanning mode with electron microscopy was employed. Considering the limit-

ations of the two lighter elements B and O in this test, the contents of the heavy elements La, Na and K were characterized.

Optical spectroscopy

The ultraviolet–visible (UV-vis) diffuse reflectance spectra of the powder KNLBO sample were acquired in the 200–1200 nm region using a Hitachi UH4150 spectrophotometer with $BaSO_4$ as a standard sample. According to the Kubelka–Munk formula,[30] the experimental energy gap of the title compound was further obtained. Meanwhile, the IR behavior of KNLBO was inspected over the test wavelength region of 500–4000 cm^{-1} with a Shimadzu IR Affinity1 spectrometer at room temperature.

Computational details

To evaluate the structure–property relationship, theoretical calculations were conducted with the plane-wave pseudopotential technique implemented in the CASTEP program *via* density functional theory (DFT) on the actual unit cell.[31] In this work, the density of states (DOS), band structure, and birefringence of KNLBO were systematically analyzed. In KNLBO, the electrons B $2s^2 2p^1$, Na $2s^2 2p^6 3s^1$, K $3s^2 3p^6 4s^1$, La $5d^1 6s^2$ and O $2s^2 2p^4$ were regarded as valence electrons. The Perdew–Burke–Ernzerhof functional within the generalized gradient approximation was chosen to process the exchange–correlation effects,[32,33] which helps to accurately capture the electronic and structural properties of KNLBO. The kinetic energy cutoff for the plane-wave basis was set to be 700 eV, and a Monkhorst–Pack *k*-point grid of 4 × 3 × 2 was employed for sampling and numerical integration in the Brillouin zone.

Results and discussion

Preparation of KNLBO

The polycrystalline KNLBO were experimentally prepared through a high-temperature solid-state reaction method. PXRD measurements were employed to check the purity of the target sample. As illustrated in Fig. 1a, the experimentally observed PXRD patterns of KNLBO agree well with those derived from the single-crystal structure, suggesting that the prepared polycrystalline samples were of pure phase. Furthermore, single crystals of KNLBO were grown by heating the compound with the optimized B_2O_3–K_2CO_3 flux system above 800 °C in a Pt crucible, followed by cooling the solution at 1–3 °C h^{-1} from 800 to 650 °C and then to ambient temperature by air cooling, as presented in Fig. S1.†

Thermal analyses

The TGA–DSC curves of the polycrystalline KNLBO from 25 to 1200 °C were analyzed, as displayed in Fig. 1b, in which no sharp peak is detected in the measured heating stage. Meanwhile, there is no distinct weight loss up to around 1050 °C in the corresponding TGA patterns, suggesting that the title compound exhibits good thermal stability. The varied temperature PXRD patterns of KNLBO were also analyzed (Fig. S2†).

Structural analysis of KNLBO

The crystal structure of KNLBO was experimentally solved for the first time. The single-crystal X-ray diffraction results demonstrated that KNLBO crystallizes into the acentric orthorhombic space group *Amm*2 with the lattice parameters a = 5.1933(6) Å, b = 11.4720(15) Å, c = 7.3074(9) Å and Z = 2, which is analogous to the shortite structure.[26] The detailed crystallographic data and structural refinement for KNLBO are provided in Table 1. In the crystal structure of KNLBO, the asymmetric unit consists of two types of B^{3+} cations, one unique La^{3+} cation, one independent K^+ and two independent Na^+ cations as well as two O^{2-} anions. As exhibited in Fig. 2a, each B atom is bonded to three O atoms and forms isolated $[BO_3]$ triangles with B–O bond distances in the region from 1.361(16) to 1.410(11) Å. With respect to the rare-earth La atoms, they

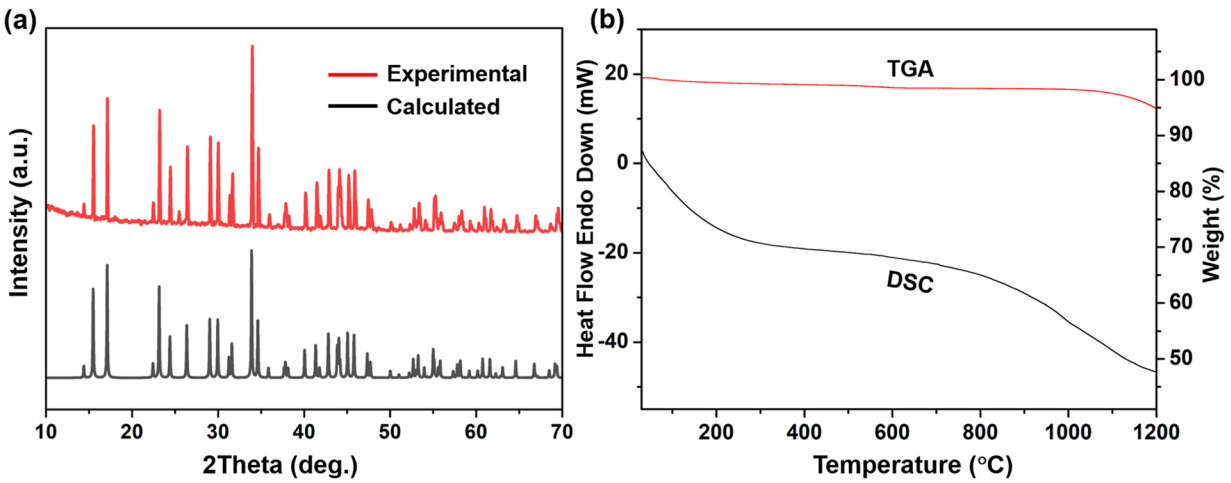

Fig. 1 (a) Standard and observed PXRD patterns of the as-synthesized KNLBO samples. (b) DSC and TGA curves for the KNLBO polycrystalline samples.

Table 1 Crystal data and structural refinement of KNLBO

Empirical formula	KNLBO
Formula weight	539.33
Temperature (K)	297 K
Crystal system	Orthorhombic
Space group	*Amm*2
a (Å)	5.1933(6)
b (Å)	11.4720(15)
c (Å)	7.3074(9)
Volume (Å^3)	435.36(9)
Z	2
Flack parameter	−0.04(5)
λ (Å)	0.71073
R (int.)	0.0424
GOF on (F^2)	1.246
Final *R* indices[a] [$F_o^2 > 2\sigma(F_o^2)$]	$R_1 = 0.0294$, $wR_2 = 0.0814$
R indices (all data)	$R_1 = 0.0306$, $wR_2 = 0.0849$
CCDC number	2265827

[a] $R_1 = \sum||F_o| - |F_c||/\sum|F_o|$; $wR_2 = [\sum w(F_o^2 - F_c^2)^2/\sum w(F_o^2)^2]^{1/2}$.

are coordinated with nine O atoms to construct a [LaO_9] basic block and the corresponding La–O bond distances vary between 2.464(2) and 2.696(3) Å. These observed values are consistent with those of other rare-earth borates.[21] To be specific, the two kinds of planar [BO_3] units with the zero-dimensional (0D) framework are parallel on the *ac* and *bc* planes (Fig. 2b), respectively, which is similar to those of [CO_3] triangles in the carbonate $Na_2Ca_2(CO_3)_3$.[26] As presented in Fig. 2c, the adjacent [LaO_9] polyhedra are connected simultaneously *via* corner and face sharing to form chains. It is clearly observed in Fig. 2d that these structural motifs of the [BO_3] and [LaO_9] groups are further decorated to yield a two-dimensional (2D) configuration *via* corner-sharing that runs parallel to the *ac* plane. Then, the neighboring layers in the *ac* plane are further stacked along the *b*-axis to build a three-dimensional (3D) configuration, as depicted in Fig. 2e. The crystallographic analysis reveals that KNLBO is structurally related to the lanthanide borate $Na_3La_2(BO_3)_3$.[24] Although they have different alkali metal cations, B^{3+} and La^{3+} cations adopt a three- and nine-coordinate environment to form isolated trigonal planar units [BO_3] and distorted polyhedra [LaO_9], respectively, which construct the orthorhombic acentric 3D framework. According to structure–property relationships,[34] such accordant arrangements of [BO_3] triangles and distorted [LaO_9] polyhedra are beneficial for generating a significant enhancement of microscopic polarizability.

EDS analysis

To further validate the identity of Na, K, La and O elements, EDS tests for the KNLBO crystal were carried out to probe the elemental ratio and distribution. The observed results demonstrated that the molar ratio of Na/K/La//O elements was found to be around 2.09/1.10/2.66/8.43 and distributed homogeneously (Fig. S3†), which is in line with the observation of the crystal structure.

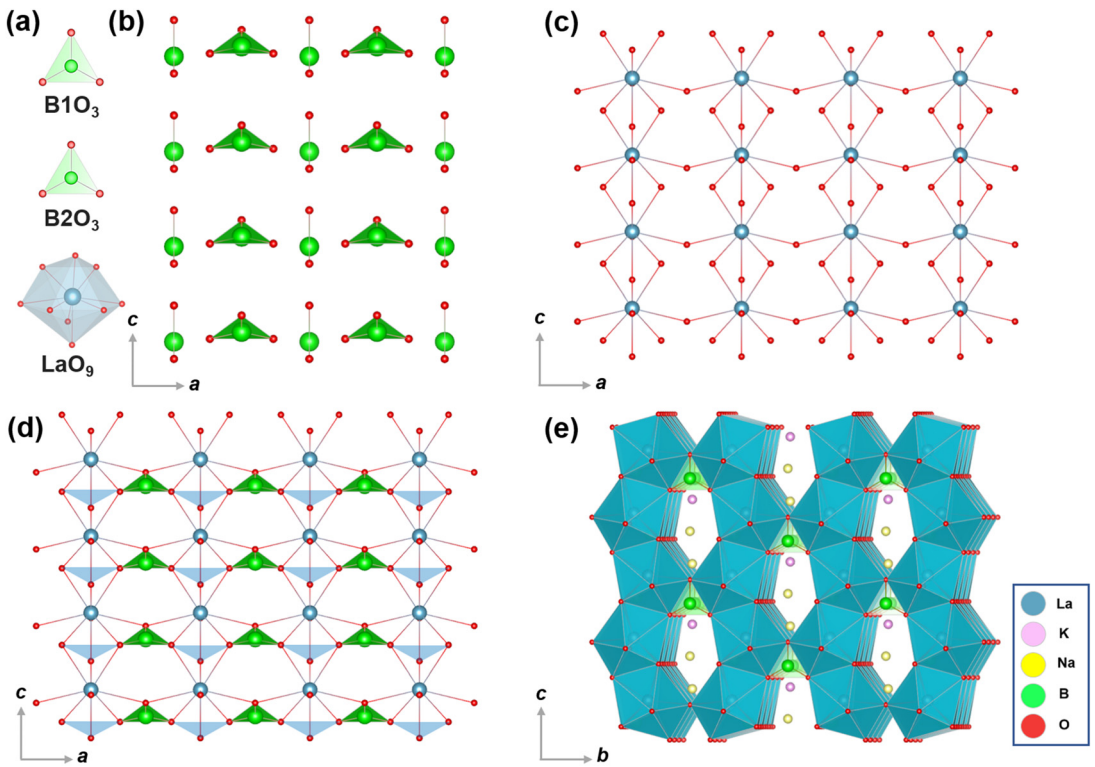

Fig. 2 Structural characterization of KNLBO. (a) The structural polyhedral representation of [$B1O_3$], [$B2O_3$] and [LaO_9]. (b and c) The spatial arrangement of the isolated [BO_3] and [LaO_9] units along the *ac* plane, respectively. (d) The 2D configuration composed of the [BO_3] and [LaO_9] groups *via* corner-sharing along the *ac* plane. (e) The 3D structural framework viewed along the *bc* plane.

Spectroscopic properties

To characterize the optical transmittance behaviors, the UV-vis-NIR diffuse reflectance spectrum was obtained from polycrystalline KNLBO, as presented in Fig. 3a, which indicates that the title compound possesses a short UV cutoff edge at around 212 nm, corresponding to a broad optical band gap of 5.30 eV based on the Kubelka–Munk formula (inset of Fig. 3a), comparable to that of $YAl_3(BO_3)_4$.[35] Accordingly, this linear optical performance indicates its potential application in the UV region. Meanwhile, the IR spectral curves of KNLBO were also measured, as plotted in Fig. 3b. According to previous reports,[21,24] the peaks observed at around 1196 cm^{-1} are mainly ascribed to the asymmetric stretching and symmetric stretching vibration modes of $[BO_3]^{3-}$ units. The peaks that emerged at 744–589 cm^{-1} predominantly correspond to the bending of the B–O groups. These observations further corroborate the existence of $[BO_3]^{3-}$ primitives and are in accordance with those suggested by the structure of KNLBO.

SHG characterization

Because this title material lacks a center of symmetry, the SHG capability of the KNLBO compound was evaluated through the modified Kurtz–Perry method under a 1064 nm pulsed laser. As depicted in Fig. 3(c and d), the strength of the SHG response for KNLBO was increased gradually with increasing particle sizes and eventually reached a maximum magnitude, displaying a phase-matching behavior. Moreover, KNLBO possesses strong SHG intensities of 2.6 × KDP and 1.4 × LBO at 1064 nm within the same particle size range of 177–210 μm. It is worth noting that its experimental SHG efficiency is comparable with those of most reported rare earth borate oxides, including $La_2CaB_{10}O_{19}$ (2 × KDP),[20] $K_5Mg_2La_3(BO_3)_6$ (3.1 × KDP),[21] $K_7PbY_2B_{15}O_{30}$ (2.1 × KDP),[22] $Na_3La_2(BO_3)_3$ (2 × KDP),[24] $YAl_3(BO_3)_4$ (3 × KDP),[35] $Na_3Y_3(BO_3)_4$ (3 × KDP),[36] and $RECa_4O(BO_3)_3$ (RE = Y, Gd) (3 × KDP).[37] This observed result is consistent with the structural features of KNLBO. Consequently, these inherent merits of the high UV transparency and a strong phase-matching SHG intensity explicitly imply that the KNLBO crystal is a good candidate for NLO applications in the UV window.

Structure–property relationship

To intuitively shed light on the structure–property relationship of KNLBO, DFT was adopted in the VASP package and theoretical calculations. The moderate calculated birefringence was determined to be 0.019 @ 1 μm, as provided in Fig. S4.† As depicted in Fig. 4a, the simulation results reveal that the valence band maximum (VBM) and the conduction band minimum (CBM) of the KNLBO crystal belong to the same position (G), implying that the title compound belongs to the direct band gap. Furthermore, the theoretical band gap of KNLBO is calculated to be approximately 4.0 eV, which is systematically smaller than the experimentally observed value. Based on the GGA approach, the represented discrepancy is normally generated by the discontinuity of the exchange–correlation function. In addition, we probed the detailed bands composed of the total and partial densities of states. It is clearly found in Fig. 4b that the electron states near the

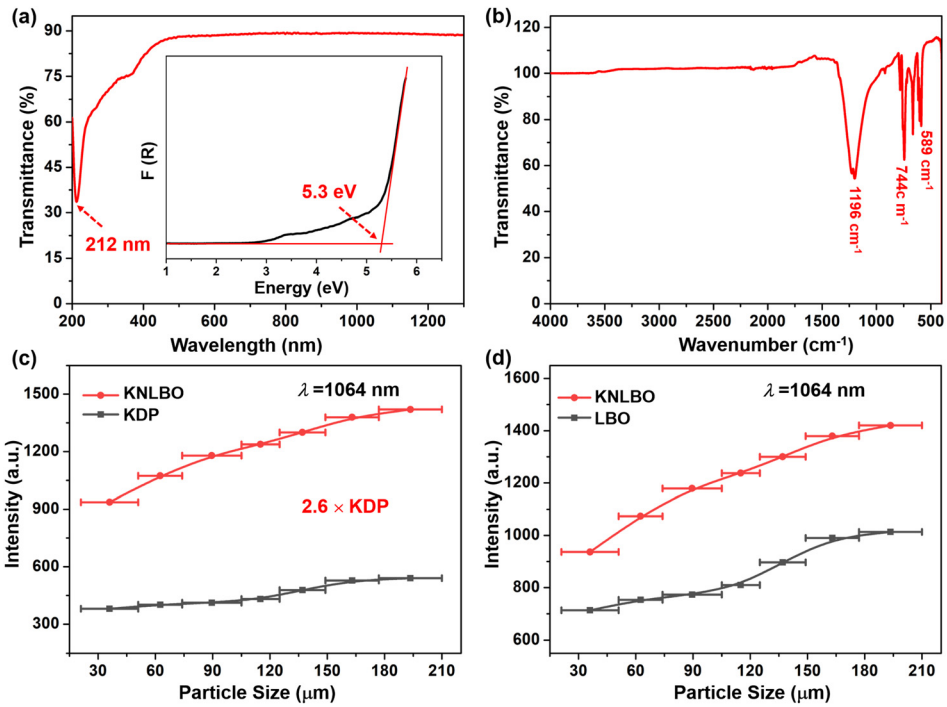

Fig. 3 Optical characterization of KNLBO. (a) UV-vis-NIR diffuse reflectance spectra with a broad band gap of 5.3 eV. (b) IR transmission spectrum. (c and d) Phase-matching SHG signals for the title compound, KDP and LBO references with 1064 nm laser radiation.

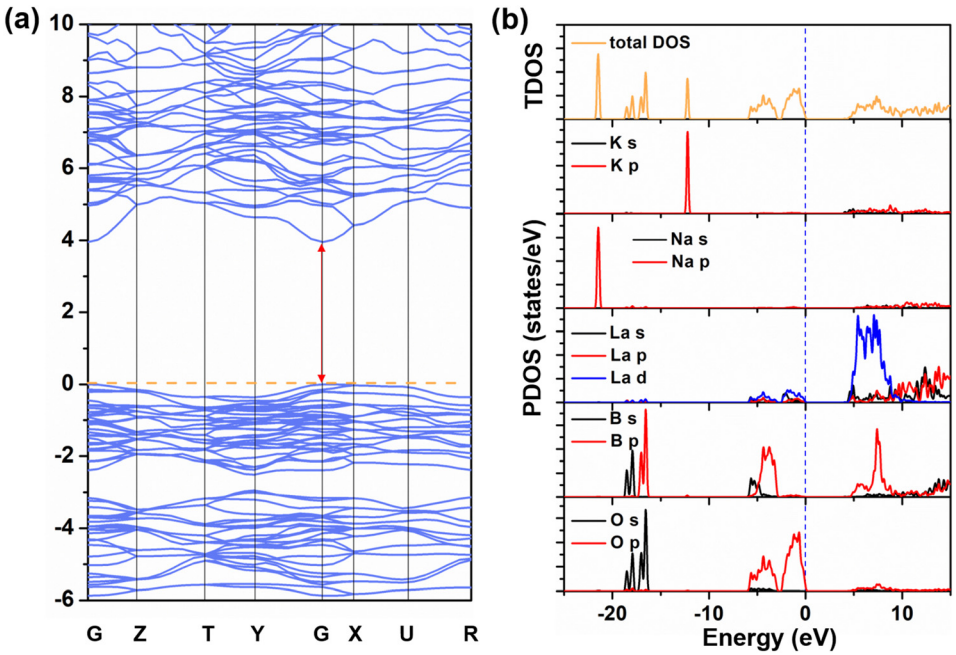

Fig. 4 (a) Calculated band structure. (b) Partial DOS of KNLBO, in which the blue dashed line represents the Fermi level.

maximum of the valence bands observed ranging from −6.0 to 0.0 eV are primarily dominated by B 2p, La 5d and O 2p orbitals, with a small amount from B 2s orbitals. The electron states near the minimum of the conduction bands observed in the range of 5–10 eV primarily correspond to the La 5d, B 2p and O 2p orbitals. Nevertheless, the contribution of the alkali metal cations K^+ and Na^+ is almost negligible. Considering that the optical properties depend mainly upon the electronic structures near the Fermi level, these observations imply that the appreciable second-order nonlinearity of the KNLBO crystal is predominantly prompted by the cooperative effects of the coplanar [BO_3] units and distortive [LaO_9] structural primitives. Therefore, we speculate that these NLO-active [BO_3] and [LaO_9] structural motifs can be extended into the design of other rare earth metal borate UV NLO crystals.

Conclusions

In summary, a novel acentric polar rare earth borate, KNLBO, was rationally designed and synthesized through a flux method. KNLBO features a three-dimensional framework constructed from isolated [BO_3] plane triangles and distorted [LaO_9] polyhedra, with Na^+ and K^+ cations residing in the cavities. The target compound possesses a short UV cutoff edge of 212 nm with an enlarged optical band gap of 5.3 eV. Furthermore, it demonstrates a strong phase-matchable SHG activity of 2.6 times that of KDP, which makes it a promising candidate for UV NLO applications. Additionally, structural and theoretical analyses suggest that the cooperative contributions of the planar [BO_3] and distorted [LaO_9] motifs are largely responsible for the significantly improved second-order nonlinearity. These findings lay a foundation for fabricating the design and exploration of novel UV NLO materials.

Conflicts of interest

There are no conflicts to declare.

Acknowledgements

This work was supported by the National Key R&D Program of China (2021YFA0717800) and the Natural Science Foundation of China (Grant No. 52002273, 52002220, 61835014 and 51890864).

References

1 D. F. Eaton, Nonlinear optical materials, *Science*, 1991, **253**, 281–287.
2 (*a*) K. M. Ok, Toward the rational design of novel noncentrosymmetric materials: factors influencing the framework structures, *Acc. Chem. Res.*, 2016, **49**, 2774–2785; (*b*) H. C. Lan, F. Liang, X. X. Jiang, C. Zhang, H. H. Yu, Z. S. Lin, H. J. Zhang, J. Y. Wang and Y. C. Wu, Pushing nonlinear optical oxides into the mid-infrared spectral region beyond 10 μm: Design, synthesis, and characterization of $La_3SnGa_5O_{14}$, *J. Am. Chem. Soc.*, 2018, **140**, 4684–4690; (*c*) M. Xia, X. Jiang, Z. Lin and R. Li, "All-three-in-one": A new bismuth–tellurium–borate Bi_3TeBO_9 exhibiting

strong second harmonic generation response, *J. Am. Chem. Soc.*, 2016, **138**, 14190–14193.

3 P. S. Halasyamani and J. M. Rondinelli, The must-have and nice-to-have experimental and computational requirements for functional frequency doubling deep-UV crystals, *Nat. Commun.*, 2018, **9**, 2972.

4 C. Wu, C. B. Jiang, G. F. Wei, X. X. Jiang, Z. J. Wang, Z. S. Lin, Z. P. Huang, M. G. Humphrey and C. Zhang, Toward large second-harmonic generation and deep-UV transparency in strongly electropositive transition metal sulfates, *J. Am. Chem. Soc.*, 2023, **145**, 3040–3046.

5 G. H. Zou and K. M. Ok, Novel ultraviolet (UV) nonlinear optical (NLO) materials discovered by chemical substitution-oriented design, *Chem. Sci.*, 2020, **11**, 5404–5409.

6 C. Y. Pan, X. R. Yang, L. Xiong, Z. W. Lu, B. Y. Zhen, X. Sui, X. B. Deng, L. Chen and L. M. Wu, Solid-state nonlinear optical switch with the widest switching temperature range owing to its continuously tunable T_c, *J. Am. Chem. Soc.*, 2020, **142**, 6423–6431.

7 (*a*) X. Jiang, S. Deng, M. Whangbo and G. Guo, Material research from the viewpoint of functional motifs, *Natl. Sci. Rev.*, 2022, **9**, nwac017; (*b*) B. W. Liu, H. Y. Zeng, X. M. Jiang and G. C. Guo, Phase matching achieved by bandgap widening in infrared nonlinear optical materials $[ABa_3Cl_2][Ga_5S_{10}]$ (A = K, Rb, and Cs), *CCS Chem.*, 2020, **2**, 964–973.

8 (*a*) W. Q. Lu, Z. L. Gao, X. T. Liu, X. X. Tian, Q. Wu, C. G. Li, Y. X. Sun, Y. Liu and X. T. Tao, Rational design of a $LiNbO_3$-like nonlinear optical crystal, Li_2ZrTeO_6, with high laser-damage threshold and wide mid-IR transparency window, *J. Am. Chem. Soc.*, 2018, **140**, 13089–13096; (*b*) H. Chen, W. B. Wei, H. Lin and X. T. Wu, Transition-metal-based chalcogenides: A rich source of infrared nonlinear optical materials, *Coord. Chem. Rev.*, 2021, **448**, 214154; (*c*) D. Wang, Y. Zhang, Q. Shi, Q. Liu, D. Yang, B. Zhang and Y. Wang, Tellurate polymorphs with high-performance nonlinear optical switch property and wide mid-IR transparency, *Inorg. Chem. Front.*, 2022, **9**, 1708–1713; (*d*) C. Li, Z. Gao, P. Zhao, X. Tian, H. Wang, Q. Wu, W. Lu, Y. Sun, D. Cui and X. Tao, Crystallographic investigations into the polar polymorphism of $BaTeW_2O_9$: Phase transformation, controlled crystallization, and linear and nonlinear optical properties, *Cryst. Growth Des.*, 2019, **19**, 1767–1777; (*e*) C. F. Sun, C. L. Hu, X. Xu, J. B. Ling, T. Hu, F. Kong, X. F. Long and J. G. Mao, $BaNbO(IO_3)_5$: A new polar material with a very large SHG response, *J. Am. Chem. Soc.*, 2009, **131**, 9486–9487.

9 (*a*) W. Zhao, C. Li, T. Han, J. Jiao, Y. She, D. Ju, F. Liang, N. Ye, Z. Hu and Y. Wu, $Cs_2Bi_2OSi_2O_7$: A promising bismuth silicate nonlinear optical crystal with face-sharing BiO_5 polyhedra exhibiting strengthened second harmonic generation response and birefringence, *Chem. Mater.*, 2022, **34**, 3365–3372; (*b*) H. W. Yu, W. G. Zhang, J. S. Young, J. M. Rondinelli and P. S. Halasyamani, Bidenticity-enhanced second harmonic generation from Pb chelation in $Pb_3Mg_3TeP_2O_{14}$, *J. Am. Chem. Soc.*, 2016, **138**, 88–91; (*c*) M. Luo, F. Liang, X. Hao, D. H. Lin, B. X. Li, Z. S. Lin and N. Ye, Rational design of the nonlinear optical response in a tin iodate fluoride $Sn(IO_3)_2F_2$, *Chem. Mater.*, 2020, **32**, 2615–2620.

10 (*a*) G. H. Zou, Z. E. Lin, H. M. Zeng, H. Jo, S. J. Lim, T. S. You and K. M. Ok, $Cs_3VO(O_2)_2CO_3$: An exceptionally thermostable carbonatoperoxovanadate with an extremely large second-harmonic generation response, *Chem. Sci.*, 2018, **9**, 8957–8961; (*b*) G. Peng, C. S. Lin and N. Ye, $NaZnCO_3(OH)$: A high-performance carbonate ultraviolet nonlinear optical crystal derived from $KBe_2BO_3F_2$, *J. Am. Chem. Soc.*, 2020, **142**, 20542–20546; (*c*) C. Wu, X. X. Jiang, Z. J. Wang, L. Lin, Z. S. Lin, Z. P. Huang, X. F. Long, M. G. Humphrey and C. Zhang, Giant optical anisotropy in the UV-transparent 2D nonlinear optical material $Sc(IO_3)_2(NO_3)$, *Angew. Chem., Int. Ed.*, 2021, **60**, 3464–3468.

11 C. Wu, X. X. Jiang, Z. J. Wang, H. Y. Sha, Z. S. Lin, Z. P. Huang, X. F. Long, M. G. Humphrey and C. Zhang, UV solar-blind region phase-matchable optical nonlinearity and anisotropy in a π-conjagated cation-containing phosphate, *Angew. Chem., Int. Ed.*, 2021, **61**, 14806–14810.

12 (*a*) M. Mutailipu, K. R. Poeppelmeier and S. L. Pan, Borates: A rich source for optical materials, *Chem. Rev.*, 2021, **121**, 1130–1202; (*b*) F. Liang, L. Kang, P. F. Gong, Z. S. Lin and Y. C. Wu, Rational design of deep-ultraviolet nonlinear optical materials in fluorooxoborates: Toward optimal planar configuration, *Chem. Mater.*, 2017, **29**, 7098–7102.

13 (*a*) M. Mutailipu, M. Zhang, Z. Yang and S. Pan, Targeting the next generation of deep-ultraviolet nonlinear optical materials: Expanding from borates to borate fluorides to fluorooxoborates, *Acc. Chem. Res.*, 2019, **52**, 791–801; (*b*) Z. J. Li, W. Q. Jin, F. F. Zhang, Z. L. Chen, Z. H. Yang and S. L. Pan, Achieving short-wavelength phase-matching second harmonic generation in boron-rich borosulfate with planar $[BO_3]$ units, *Angew. Chem., Int. Ed.*, 2021, **61**, e202112844.

14 C. T. Chen, G. L. Wang, X. Y. Wang and Z. Y. Xu, Deep-UV nonlinear optical crystal $KBe_2BO_3F_2$—Discovery, growth, optical properties and applications, *Appl. Phys. B: Lasers Opt.*, 2009, **97**, 9–25.

15 S. G. Zhao, P. F. Gong, L. Bai, X. Xu, S. Q. Zhang, Z. H. Sun, Z. S. Lin, M. C. Hong, C. T. Chen and J. H. Luo, Beryllium-free $Li_4Sr(BO_3)_2$ for deep-ultraviolet nonlinear optical applications, *Nat. Commun.*, 2014, **5**, 4019.

16 H. P. Wu, S. L. Pan, K. R. Poeppelmeier, H. Y. Li, D. Z. Jia, Z. H. Chen, X. Y. Fan, Y. Yang, J. M. Rondinelli and H. S. Luo, *J. Am. Chem. Soc.*, 2011, **133**, 7786–7790.

17 H. Wu, H. Yu, W. Zhang, J. Cantwell, K. R. Poeppelmeier, S. Pan and P. S. Halasyamani, Top-seeded solution crystal growth and linear and nonlinear optical properties of $Ba_4B_{11}O_{20}F$, *Cryst. Growth Des.*, 2017, **17**, 1404–1410.

18 M. Mutailipu, M. Zhang, H. P. Wu, Z. H. Yang, Y. H. Shen, J. L. Sun and S. L. Pan, $Ba_3Mg_3(BO_3)_3F_3$ polymorphs with reversible phase transition and high performances as ultra-

violet nonlinear optical materials, *Nat. Commun.*, 2018, **9**, 3089.

19 Z. X. Chen, C. Y. Zhao, X. H. Li, W. D. Yao, W. L. Liu and S. P. Guo, $KREP_2Se_6$ (RE = Sm, Gd, Tb): The first rare-earth selenophosphates with remarkable nonlinear optical activities realized by synergistic effect of RE- and P-based motifs, *Small*, 2023, **19**, 2206910.

20 Y. C. Wu, J. G. Liu, P. Z. Fu, J. X. Wang, H. Y. Zhou, G. F. Wang and C. T. Chen, New lanthanum and calcium borate $La_2CaB_{10}O_{19}$, *Chem. Mater.*, 2001, **13**, 753–755.

21 R. Liu, H. Wu, H. Yu, Z. Hu, J. Wang and Y. Wu, $K_5Mg_2La_3(BO_3)_6$: An efficient deep-ultraviolet nonlinear optical material, *Chem. Mater.*, 2021, **33**, 4240–4246.

22 Z. Xie, M. Mutailipu, G. He, G. Han, Y. Wang, Z. Yang, M. Zhang and S. Pan, A series of rare-earth borates $K_7MRE_2B_{15}O_{30}$ (M = Zn, Cd, Pb; RE = Sc, Y, Gd, Lu) with large second harmonic generation responses, *Chem. Mater.*, 2018, **30**, 2414–2423.

23 X. P. Shi, A. Tudi, M. Cheng, F. F. Zhang, Z. H. Yang, S. J. Han and S. L. Pan, Noncentrosymmetric rare-earth borate fluoride $La_2B_5O_9F_3$: A new ultraviolet nonlinear optical crystal with enhanced linear and nonlinear performance, *ACS Appl. Mater. Interfaces*, 2022, **14**, 18704–18712.

24 (*a*) G. C. Zhang, Y. C. Wu, P. Z. Fu, G. F. Wang, S. L. Pan and C. T. Chen, A new nonlinear optical borate crystal $Na_3La_2(BO_3)_3$, *Chem. Lett.*, 2001, **30**, 456–457; (*b*) K. Li, G. C. Zhang, S. Guo, X. Zhang, R. He, J. X. Zhang, Z. S. Lin and Y. C. Wu, Linear and nonlinear optical properties of $Na_3La_2(BO_3)_3$ crystal, *Opt. Laser Technol.*, 2013, **54**, 407–412.

25 R. Hoppe and M. Miessen, Z. Neue Borate der Alkalimetalle: $KNa_2[BO_3]$, *Anorg. Allg. Chem.*, 1984, **518**, 55–64.

26 B. Dickens, A. Hyman and W. Brown, Crystal structure of $Ca_2Na_2(CO_3)_3$ (shortite), *J. Res. Natl. Bur. Stand., Sect. A*, 1971, **75**, 129.

27 S. K. Kurtz and T. T. Perry, A powder technique for the evaluation of nonlinear optical materials, *J. Appl. Phys.*, 1968, **39**, 3798–3813.

28 G. M. Sheldrick, *SHELXS-97: Program for the Solution of Crystal Structures*, University of Göttingen, Germany, 1997.

29 A. L. Spek, Single-crystal structure validation with the program PLATON, *J. Appl. Crystallogr.*, 2003, **36**, 7–13.

30 P. Kubelka and F. Z. Munk, Ein Beitrag zur Optik der Farbanstriche (Contribution to the optic of paint), *Z. Technol. Phys.*, 1931, **12**, 593.

31 J. P. Perdew, A. Ruzsinszky, G. I. Csonka, O. A. Vydrov, G. E. Scuseria, L. A. Constantin, X. Zhou and K. Burke, Restoring the density-gradient expansion for exchange in solids and surfaces, *Phys. Rev. Lett.*, 2008, **100**, 136406.

32 J. P. Perdew, K. Burke and M. Ernzerhof, Generalized gradient approximation made simple, *Phys. Rev. Lett.*, 1996, **77**, 3865–3868.

33 J. P. Perdew and Y. Wang, Pair-distribution function and its coupling-constant average for the spin-polarized electron gas, *Phys. Rev. B: Condens. Matter Mater. Phys.*, 1992, **46**, 12947–12954.

34 C. Wu, G. Yang, M. G. Humphrey and C. Zhang, Recent advances in ultraviolet and deep-ultraviolet second-order nonlinear optical crystals, *Coord. Chem. Rev.*, 2018, **375**, 459–488.

35 R. He, Z. S. Lin, M. H. Lee and C. T. Chen, Ab initio studies on the mechanism for linear and nonlinear optical effects in $YAl_3(BO_3)_4$, *J. Appl. Phys.*, 2011, **109**, 103510.

36 F. Shan, L. Kang, G. Zhang, J. Yao, Z. Lin, M. Xia, X. Zhang, Y. Fu and Y. Wu, $Na_3Y_3(BO_3)_4$: A new non-centrosymmetric borate with an open-framework structure, *Dalton Trans.*, 2016, **45**, 7205–7208.

37 M. Iwai, T. Kobayashi, H. Furuya, Y. Mori and T. Sasaki, Crystal growth and optical characterization of rare-earth (Re) Calcium oxyborate $ReCa_4O(BO_3)_3$ (Re = Y or Gd) as new nonlinear optical material, *Jpn. J. Appl. Phys.*, 1997, **36**, L276.